dcis2011
26th Conference on Design of Circuits and Integrated Systems
The next 25 years

A Methodology to Test a Stent-Graft Endoleakage Monitor

Cristina Oliveira
Faculdade de Engenharia, U. Porto, Portugal
coliveiracris@gmail.com

José Machado da Silva
INESC Porto, Faculdade de Engenharia, U. Porto, Portugal
jms@fe.up.pt

Luís A. Rochaz
I3N/IPC Instituto de Nanoestruturas, Nanomodelação e Nanofabricação, U. Minho, Portugal
lrocha@dei.uminho.pt

***Abstract*—A new inductive coupling based wireless system is being developed to monitor the condition status of aortic stent-grafts. It relies on the measure of the stent-graft's outer pressure using a capacitive sensor placed in a LC resonant circuit. The work presented herein addresses the testing of the LC sensor circuit to diagnose whether observed pressure deviations are due to defects occurring in the sensor's inductor and capacitor or to an actual degradation of the stent-graft.**

I. Introduction

An abdominal aortic aneurysm is a localized widening (dilation) of the aorta resulting from a loss of strength of the vessel's walls. The treatment of this dangerous weakness by means of surgical reconstruction, though effective, is nevertheless responsible for a significant morbidity and mortality rate (3% to 7%) [1].

Endovascular stent grafting provides a less invasive and safer treatment in many cases. However, in spite of improvement of stent-grafts' technology, deficient healing between the grafts and the blood vessels may lead to several problems. Reintervention after endovascular repair (EVAR) of abdominal aortic aneurysms (AAAs) is required in up to 10% of patients until 30 days after the first intervention [2]. Traditional stent-graft monitoring include computed tomography (CT) and magnetic resonance imaging (MRI) [2]–[4]. These are expensive, raise risks to patients' health, and may be incompatible with some stent-grafts technologies. Some other proposed methods present less health impacts, but many of them require some degree of surgical invasion [2], [3] and take long time to be performed, leading in some cases to false positive findings [5].

Despite improvements in stent-grafts over the last decade one of the most frequent complications is still the occurrence of endoleaks [6]. These are defined as the persistence of blood flow outside the lumen of the endoluminal graft but within the aneurysm sac and can be identified in 15% to 52% of patients after endovascular repair. Often the pressure in the aneurysm sac in patients with an endoleak is the same as systemic arterial pressure, raising concerns of possible aneurysm enlargement and rupture. The need for monitoring intrasac pressure after endovascular repair is widely accepted, and there is currently great interest in the possibility of intraprocedurally implanting sac pressure sensors that can subsequently be interrogated remotely either intermittently or continuously. The sensor would measure the pressure within aneurysm thrombus around itself.

A. Remote Monitoring System

A wireless based endoleakage monitoring system is being developed which allows avoiding additional intervention after the first EVAR. The monitoring principle is based on the detection of pressure variations within the aneurysm sac by means of a cluster of capacitive pressure sensors attached to the stent-graft (figure 1). Each sensor comprises an LC resonant circuit, whose oscillation frequency is sensitive to pressure variations. An external reader delivers energy and detects sensor's resonance frequency through an inductive-coupling link.

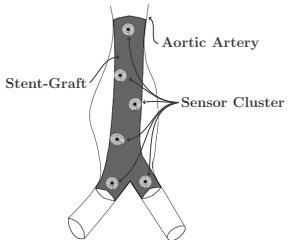

Figure 1: Sensor cluster in an abdominal aorta stent-graft.

The use of passive resonant LC sensors and their inductive-coupling based reading and powering by has been explored as a means for monitoring different processes [7]–[11]. A transformer is commonly used to model the established communication link 2. The secondary circuit includes a parallel resonant loop formed by the pressure sensitive capacitor C_s and inductor L_s. R_p and R_s model inductors parasitic series resistances, and R_{vs} represents the voltage source v_{vs} internal resistance. Figure 2 shows the resulting circuit when the transformer is replaced by its T equivalent version. Inductor L_m represents the mutual inductance created between the primary and secondary windings. It is determined by L_p and L_s inductors' values and on the magnetic coupling which depends on the distance and the medium existing between them. The use of a group of sensors placed in the same stent-graft maximizes the system sensitivity to leakages, which is an advantage comparing to the system presented in [5] which uses only one sensor. The communication with the sensor cluster uses the 12.5 MHz to 20.0 MHz frequency band, specifically allocated for use in medical applications [12].

Despite conceptual simplicity, this monitoring system presents actually some technical challenges. Since the sensor

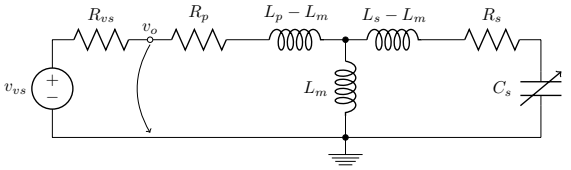

Figure 2: T equivalent model of the inductive-coupling.

circuit is powerless the operating energy needs to be transmitted via inductive-coupling. This and the communication efficiency are affected by the type and thickness of the biological tissue transmission medium. An important aspect to be considered concerns the frequency shift due to the sensor's inductor bending after placement in the stent. Consequently the corresponding inductance can change [13] due to bending. This deformation may have a direct impact on variations of the sensor's oscillation frequency, producing uncertainty in the pressure detection.

The reading process is commonly based on the measurement of the transformer's input impedance with a network analyzer, after which one extracts the sensor capacitance value. The approach being used here relies on the direct analysis of LC's resonant frequency. This allows decreasing the sensitivity to angle misalignments between the two inductors. However, interpreting the captured oscillation frequency cannot be made in a simple single observation. The pressure in the stent-graft varies periodically with the arterial blood pressure. In consequence, what one actually captures is a distribution of resonant frequencies, modulated, on one hand, by the cardiac beating (60 to 100 beats per minute for a healthy heart) and the range of pressures it generates. On the other hand, the frequency is also affected by the operating condition status of the pressure sensor. Therefore, in case an abnormal resonant frequency distribution is observed how can one distinguish a defective stent-graft from a defective sensor? The work presented here addresses this problem in order to improve the reliability of the proposed endoleakage monitor.

II. A Differential Reading Approach

The resistive elements in the model shown in figure 2 can be ignored in the calculation of the oscillation frequency. If the mutual inductance L_m is replaced by $k\sqrt{L_p L_s}$, k being the magnetic coupling factor, the equivalent inductance can be described as $L_{eq} = (1-k^2)L_s = (L_s - L_m) + (L_p - L_m)\|(L_m)$, and then one obtains equation 1 for the equivalent natural frequency of the resonant LC circuit.

Figure 3 shows the variation of the oscillation frequency using three different approaches: equation 1, Agilent ADS simulations, and by means of the transfer function of the circuit presented in figure 2. One can see that the oscillation frequency shifting due to k variations is relatively small, particularly if k is smaller than 0.1 – in fact that is the case for the sensors placed a few centimetres underneath the skin in an environment comprising biological tissue [14].

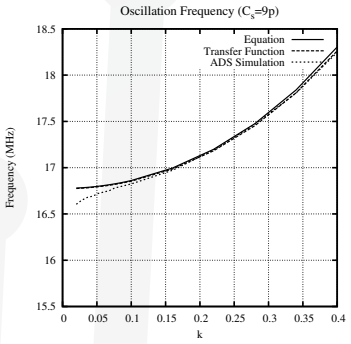

Figure 3: Variation of oscillation frequency with k.

$$f_{osc} = \frac{1}{2\pi\sqrt{(1-k^2)L_s C_s}}. \quad (1)$$

A reader circuit based on the inductive coupling presented in figure 2 has some limitations regarding signal's quality. Since the captured signal has a very small amplitude, it is difficult to differentiate it from noise and harmonics. A new circuit has been developed (figure 4) which resorts to a twin circuit added to the first part of the reader in order to provide a differential detection of the reflected oscillation. By duplicating the undesired signal the common-mode noise is also eliminated, increasing the output signal's quality.

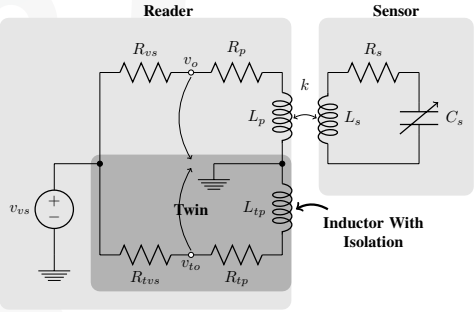

Figure 4: Remote pressure variation detector circuit.

Equation 2 gives the transfer function found between voltages v_{vs} and v_o when a capacitor is placed between v_o and ground. This corresponds to a band-pass filter function that converts into a low-pass filter (eq. 3 and figure 5) if R_s is small, which is actually an objective. Both the natural frequency and quality factor of this function depend on the stimulus generator internal resistance R_{vs}. The higher this resistance the wider and flatter the passing band of this function becomes. Figure 5 shows the transfer characteristic obtained with a value of $R_{vs} = 1k\Omega$. This allows for reducing the variation of the detected oscillation frequency with the coupling factor and provides a means to minimizing amplitude variation when different frequencies are to be detected in a specified bandwidth.

$$\frac{V_o}{V_s}(s) = \frac{sL_mR_{vs}}{R_pR_s + R_sR_{vs} + s(C_pR_pR_sR_{vs} + L_pR_s + L_sR_p + L_sR_{vs}) + } (...)$$
$$(...)\frac{}{+s2(C_pL_sR_pR_{vs} + C_pL_pR_{vs}R_s + L_pL_s - L_m2) + s3(C_pL_pL_sR_{vs} - C_pR_{vs}L_m2)} \quad (2)$$

$$\frac{V_o}{V_s}(s) = \frac{L_mR_{vs}}{L_sR_p + L_sR_{vs} + s(C_pL_sR_pR_{vs} + L_pL_s - L_m2) + s2(C_pL_pL_sR_{vs} - C_pR_{vs}L_m2)} \quad (3)$$

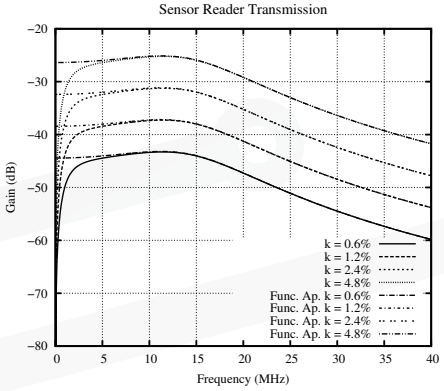

Figure 5: Transmission gain frequency responses for different coupling coefficients given by the third order function and it's second order approximation.

III. Fault detection

As this detection process provides an indirect pressure measurement, the occurrence of defects in the capacitor may mask the detection of anomalies in the stent-graft. Possible capacitor defects could be: a capacitor stuck at a constant value, a reduction of capacitor's nominal measurement range, a large deviation of capacitor's nominal value, and a collapsed capacitor. A stuck capacitor would lead to a constant resonant frequency measurement; a reduction of capacitor's nominal measurement range would allow detecting pressure deviations but these could be taken as still admissible; a large deviation of capacitor's nominal value could lead to a false defective stent-graft detection (e.g. a leaking stent-graft); and a collapsed capacitor would show no oscillation frequency. The work presented herein addresses the implementation of additional measurements and operations which allow diagnosing the occurrence of defects in the LC sensor.

The aortic blood pressure (ABP) waveform (figure 6) conveys information about the cardiovascular system such as heart rate, systolic, diastolic and mean arterial pressures. Moreover it provides information on possible complications in the endovascular stent-graft. Reading the stent-graft pressure (LC resonant frequency) at a 100-200 Hz sampling frequency allows reconstructing the ABP signal for future features extraction.

When the sensor is calibrated and ready to be placed around the stent-graft all the circuit elements (Ls, Rs and Cs) values are known. However, these components' performance may change overtime due to bend, wear and friction. In cases where the measured ABP is outside the nominal range, distinguishing that these values are caused by the pressure applied on the stent and not due to changes in the sensor components' values are of utmost importance.

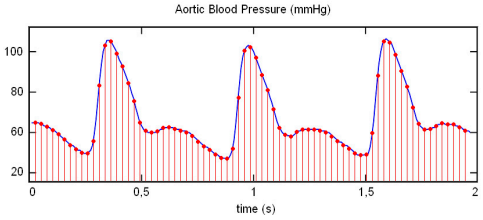

Figure 6: Aortic blood pressure waveform.

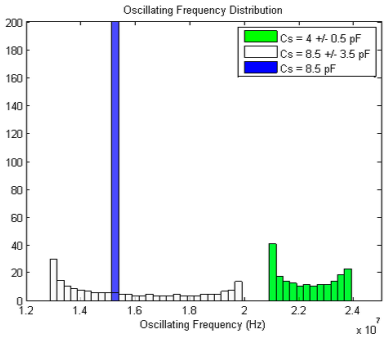

Figure 7: Distributions of good and degraded stent-graft pressure measurements.

The set of resonant frequencies captured during a number of ABP cycles allows to build an histogram of the captured values distribution. The shape of this histogram is a preliminary indicator of the occurrence of anomalies. Figure 7 shows three distributions obtained with a signal that mimics the ABP waveform – the nominal case ($C_s = 8.5 \pm 3.5$ pF) and two defects ($C_s = 4 \pm 0.5$ pF and $C_s = 8.5$ pF). Just from the observation of the defective distributions one cannot infer whether the defect has occurred in the stent-graft or in the sensor.

A. System Description

To distinguish between each possible situation, one can resort to the measure of the power transmission from the sensor to the reader circuit, as well as of the impedance seen at node $v_o(\omega)$. These additional measurements combined with the measured oscillating frequency enable the determination of the circuit components values.

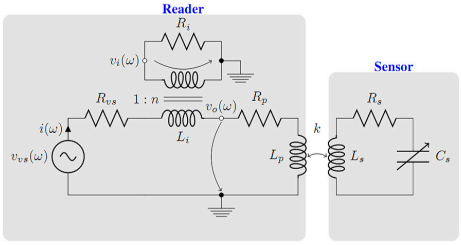

Figure 8: Circuit used to measure coupling power and impedance.

Using the circuit presented in figure 8 one can perform a frequency sweep to obtain the characteristics of input impedance (Z_L) and power (P) as functions of frequency – power is proportional to the product of $v_o(\omega)$ and $v_i(\omega)$ and $Z_L = \frac{v_o}{v_i} nR_i$. With m frequency sweeps one can obtain the inductive coupling power spectrum (figure 9) which allow us to obtain the quality factor ($Q = \frac{1}{R_s}\sqrt{\frac{L_s}{C_s}}$) of the resonant circuit.

$$\overline{P} = \frac{1}{m}\sum_{j=0}^{m} v_o(\omega) i(\omega) \equiv \frac{1}{m}\sum_{j=0}^{m} \frac{v_o(\omega) v_i(\omega)}{nR_i} \tag{4}$$

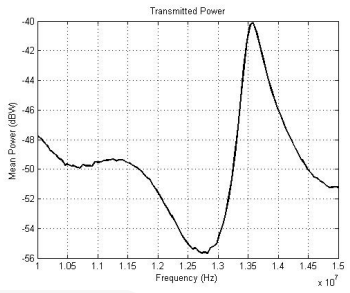

Figure 9: Mean transmitted power.

The real and imaginary parts of the impedance obtained from the frequency sweep (figure 10) are given by equations 5.

Once power and impedance measurements have been performed, one can estimate preliminary values for the coupling factor k and R_s, using f_o and Q equations and the nominal L_s and C_s values as a first guess ("seed") values. The L_s and C_s values are then estimated by means of a fitting process of the measured impedance real and imaginary parts to equations 5. This process is then iterated until a specified estimation error (difference between measured and estimated

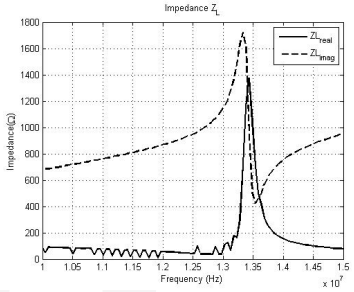

Figure 10: Real and imaginary parts of impedance Z_L.

resonant frequencies) is verified. The following pseudo-code summarizes this approach.

```
Introduce the estimated values
start_points =
=[k=0.06, Rs=50, Cs=8.5e-12, Ls=12.5e-6]
  WHILE (abs(fo_meas-fo_calc))>f_step
    k_iter = 1-1/2*pi*fo_meas*sqrt(1/Ls*Cs)
    Rs_iter = 1/Q_meas*sqrt(Ls/Cs)
    k = k_iter
    Rs = Rs_iter
    FUNCTION curvefitting(ZL_real, ZL_imag)
        estimate Ls_iter
        estimate Cs_iter
        Ls=Ls_iter
        Cs=Cs_iter
    fo_calc=1/2*pi*sqrt(Ls*Cs*(1-k^2))
  END
```

This data modelling assumes capacitor's value Cs remains constant during the measurements but in a real time measurement it varies with the pressure inside the aneurysm sac. A sequence of operations must be performed in order to acquire the needed data (transmitted power and impedance) during a time interval corresponding to a known pressure when the capacitor has a low variability (figure 11). The telemetry system comprises an electrocardiogram (ECG) equipment to record a real time electrocardiogram and the fault detection circuit to measure the transmitted power and impedance. The ECG acquisition has two purposes, the assessment of the patient's cardiac condition and to provide the fault detection triggering signal. The ECG is a widely used exam in patients with diseases associated with cardiac function, and is an important factor in the determination of risk of open surgery and EVAR [15]. To guarantee that the transmitted power and impedance measurements are carried out during a period when the capacitance is almost constant, the measurements must start in the onset of the systolic pressure and stop when the blood pressure drops again. The systole occurs around 0.2s after the contraction of the ventricles (QRS complex), so if the ECG is recorded in real time it is possible to determine the QRS occurrence and start the fault detection measurements during the systole. Then, the recorded transmitted power and impedance are used for the data modelling to extract the nominal values of the sensor's components. With this approach

$$\mathcal{R}(Z_L) = R_p + \frac{\omega^4 R_s L_m^2 C_s^2}{1+\omega^2(R_s^2C_s^2 - 2L_sC_s) + \omega^4 L_s^2 C_s^2}$$
$$\mathcal{I}(Z_L) = \omega(L_p - L_m) + \frac{\omega L_m + \omega^3(R_s^2 L_m C_s^2 + L_m^2 C_s - 2L_s L_m C_s) + \omega^5 C_s^2(L_s^2 L_m - L_m^2 L_s)}{1+\omega^2(R_s^2C_s^2 - 2L_sC_s) + \omega^4 L_s^2 C_s^2} \quad (5)$$

the small variability of the capacitor sensor is assured and the signal acquisition is carried-out during the most critical situation when the pressure is maximum. The fault detection system enables the assessment of sensor's components values and, depending on the fault gravity, it could help recalibrate the reading system so the sensor's readings are used instead of its dismissal.

B. Simulation Results

If the measured oscillating frequency is higher or lower than the expected one, it is possible to estimate the sensor's components values to make sure the frequency shift was caused by the pressure sensor and not by an eventual change of the inductor value. This situation was simulated using Agilent ADS to obtain the corresponding transmitted power and impedance curves for R_s = 12 Ω, L_s = 10 μH, k=0.1 and the sensor's capacitance C_s was varied to evaluate the fitting algorithm performance. The initial guesses were R_s = 12 Ω, L_s = 10 μH, C_s = 10 pF and k=0.1. The estimated nominal values for the circuit components are presented in table I for three different C_s expected values.

Table I: Simulation results obtained for different capacitance values.

Est \ Exp	C_s=5 pF	C_s=10 pF	C_s=15 pF
R_s (Ω)	9.7 (19.5%)	11.7 (2.9%)	11.8 (1.9%)
L_s (H)	1e-5 (0%)	1e-5 (0%)	1e-5 (0%)
C_s (F)	5.02e-12 (.37%)	1e-11 (.19%)	1.5-11 (.11%)

C. Experimental Results

An experimental set-up was used to evaluate the concept. It comprises a PCB circuit with a planar rectangular inductor, a resistor and a capacitor emulating the LC sensor. Another PCB mounted inductance acts as the primary winding. A signal generator provides a frequency sweeping of a sinewave, being a GPIB controlled data acquisition system used to capture node voltages vi and vo (figure 8). ECG and ABP signals from the MGH/MF Waveform Database [16] are used to synchronize data capture triggering. The Pan-Tompkins algorithm is used to filter the ECG signal and detect the QRS complexes [17].

After a few seconds of calibration the system is ready to start the frequency sweeping. The measurements must be done in 0.2s (duration of systole) and the system resolution, i.e. the minimum Cs and Ls detectable deviations, is dependent on the number of points (frequencies) that can be measured within this period. A MatLab script is used to control the GPIB connected devices, the detection of QRS complex in the ECG, to calculate the primary impedance and transmitted power after the captured raw data, and to estimate Cs, Ls and Rs using a data fitting based algorithm.

Table II shows results obtained for R_s=12 Ω, L_s=45.8 μH, a coupling factor k around 0.1 (set by proper separation between inductors), and for two different C_s values. The initial guesses for the fitting algorithm were R_s = 12 Ω, L_s = 45 μH, C_s = 10 pF and k=0.1.

Table II: Experimental results obtained for different capacitance values.

Est \ Exp	C_s=3.68 pF	C_s=3.9 pF
L_s (H)	4.5e-5 (1.7%)	4.5e-5 (1.7%)
C_s (F)	3.12e-12 (15%)	3.35e-12 (14%)

The fault detection approach allows detecting a shift in the sensor's capacitance C_s although the error was considerable. A possible reason for the fitting algorithm difficulty to estimate a C_s value closer to the expected is the noise associated with the frequency sweeping process. Considering the case of a cluster of sensors one can take advantage of data fusion to improve diagnosis. In this case, if a sensor provides a high pressure reading due to a endoleak or endotension episode the surrounding sensors must also show an increase on the measured pressure, but if only a sensor has an abnormal reading (extremely high or low pressure compared with the other sensors' readings) then this sensor is faulty and its readings should be ignored.

IV. Conclusions and Future Work

A methodology for testing and diagnosing failures in a inductive-link based aortic stent-graft monitoring system has been proposed. This telemetry system allows detecting endoleaks in aortic stent-grafts with increased detection effectiveness. This detection is performed after the measurement of the aneurysm sac pressure resorting to the placement of LC cells in the stent-grafts fabrics, whose resonant frequency is determined by the variations of the capacitive pressure sensor. An inductive-coupling link is used to stimulate and detect the oscillating signal. Nevertheless, as this is an indirect pressure measurement based approach, detection uncertainty is prone to occur since variations can be caused either by endoleaks in the stent-graft or due to degradation of the LC sensor performance. The work presented here addresses a methodology to diagnose deviations in the LC values after measurements of the detected signal power and inductive-coupling impedance. Preliminary experimental results show that both L and C values can be estimated with good accuracy.

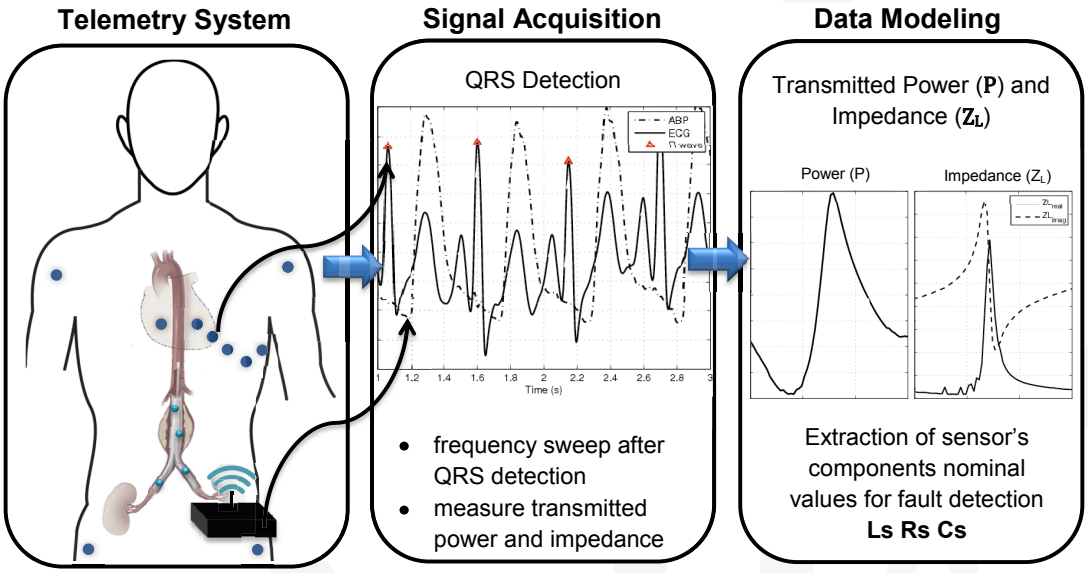

Figure 11: Fault detection block diagram.

Acknowledgments

This work has been carried-out in the framework of projects EDAM-SenseCardioHealth and Eureka/Catrene TOETS CT302, with the support of programme MIT|Portugal, Fundaï¿½ï¿½o para a Ciï¿½ncia e a Tecnologia, grant MIT-Pt/EDAM-EMD/0007/2008.

References

[1] J. van der Bas, P. Quax, A. van den Berg, V. van Hinsbergh, and J. van Bockel, "Ingrowth of aorta vascular cells into basic fibroblast growth factor-impregnated vascular prosthesis material: A porcine and human in vitro study on bood vessel prosthesis healing," *Journal of Vascular Surgery*, vol. 36, no. 6, pp. 1237–1247, 2002.

[2] L. Biasi, T. Ali, R. Hinchliffe, R. Morgan, I. Loftus, and M. Thompson, "Intraoperative dynaCT detection and immediate correction of a type 1a endoleak following endovascular repair of abdominal aortic aneurysm." *Cardiovasc Intervent Radiology*, vol. 32, no. 3, pp. 535–538, 2009.

[3] I. Nordon, A. Karthikesalingam, R. Hinchliffe, P. Holt, I. Loftus, and M. Thompson, "Secondary interventions following endovascular aneurysm repair (EVAR) and the enduring value of graft surveillance," *European Journal of Vascular and Endovascular Surgery*, vol. In Press, Corrected Proof, p. 8, 2009.

[4] B. J. Manning, S. M. O'Neill, S. N. Haider, M. P. Colgan, P. Madhavan, and D. J. Moore, "Duplex ultrasound in aneurysm surveillance following endovascular aneurysm repair: a comparison with computed tomography aortography," *Journal of Vascular Surgery*, vol. 49, no. 1, pp. 60–65, 2009.

[5] T. Ohki, K. Ouriel, P. G. Silveira, B. Katzen, R. White, F. Criado, and E. Diethrich, "Initial results of wireless pressure sensing for endovascular aneurysm repair: The apex trial–acute pressure measurement to confirm aneurysm sac exclusion," *Journal of Vascular Surgery*, vol. 45, no. 2, pp. 236–242, 2007.

[6] F. Springerand, R. W. Günther, and T. Schmitz-Rode, "Aneurysm Sac Pressure Measurement with Minimally Invasive Implantable Pressure Sensors: An Alternative to Current Surveillance Regimes after EVAR?" *Cardiovasc Intervent Radiol*, vol. 31, no. 3, pp. 460–467, 2008.

[7] M. Yvanoff, L. Fuller, and J. Venkataraman, "Implantable micro-transceiver wireless link for intra-ocular pressure measurement," *Proceedings of the IEEE Antennas and Propagation Society International Symposium*, pp. 3201–3204, 2007.

[8] M. Nabipoor and B. Majlis, "A new passive telemetry LC pressure and temperature sensor optimized for TPMS," *Journal of Physics: Conference Series*, vol. 34, no. 1, pp. 770–775, 2006.

[9] K. Fotopoulou and B. Flynn, "Wireless powering of implanted sensors using RF inductive coupling," *Proceedings of IEEE Sensors*, pp. 765–768, 2006.

[10] M. A. Fonseca, "Polymer/ceramic wireless MEMS pressure sensors for harsh environments: High temperature and biomedical applications," Ph.D. dissertation, Georgia Institute of Technology, 2007.

[11] T. Harpster, S. Hauvespre, M. Dokmeci, and K. Najafi, "A passive humidity monitoring system for in situ remote wireless testing of micropackages," *Journal of Microelectromechanical Systems*, vol. 11, no. 1, pp. 61–67, 2002.

[12] eu, "The European table of frequency allocations and utilizations in the frequency range 9 KHz to 3000 GHz," Electronic Communications Commitee (ECC), Tech. Rep., 2009.

[13] S. Leung and D. Lam, "Performance of printed polymer-based RFID antenna on curvilinear surface," *IEEE Transactions on Electronics Packaging Manufacturing*, vol. 30, no. 3, pp. 200–205, Jul. 2007.

[14] M. Sawan and B. Gosselin, "Cmos circuits for biomedical implantable devices," in *VLSI Circuits for biomedical Applications*, K. Iniewski, Ed. Artech House, 2008, ch. 3, pp. 45–51.

[15] D. C. Brewster and et. al, "Guidelines for the treatment of abdominal aortic aneurysms: Report of a subcommittee of the joint council of the american association for vascular surgery and society for vascular surgery," *Journal of Vascular Surgery*, vol. 37, no. 5, pp. 1106–1117, May 2003.

[16] A. L. Goldberger, L. A. N. Amaral, L. Glass, J. M. Hausdorff, P. C. Ivanov, R. G. Mark, J. E. Mietus, G. B. Moody, C.-K. Peng, and H. E. Stanley, "PhysioBank, PhysioToolkit, and PhysioNet: Components of a new research resource for complex physiologic signals," *Circulation*, vol. 101, no. 23, pp. e215–e220, 2000 (June 13), circulation Electronic Pages: http://circ.ahajournals.org/cgi/content/full/101/23/e215.

[17] P. J. and T. W. J., "A real-time qrs detection algorithm," *Biomed. Eng.*, vol. BME-32, no. 3, pp. 230–236, Mar. 1985.